Resonant generation of coherent LO phonons by charge oscillations in a biased quantum well

T. Papenkort* and T. Kuhn
Institut für Festkörpertheorie, Westfälische Wilhelms-Universität Münster, Wilhelm-Klemm-Straße 10, 48149 Münster, Germany

V. M. Axt
Institut für Theoretische Physik III, Universität Bayreuth, 95440 Bayreuth, Germany

(Received 8 March 2010; revised manuscript received 29 April 2010; published 26 May 2010)

A theoretical analysis of the generation of coherent and incoherent LO phonons after optical excitation of an electrically biased quantum well is presented. We show numerical calculations based on the density-matrix formalism where both coherent and incoherent phonons are included on a fully quantum kinetic level. Bulk phonon modes are used as is appropriate for the wide quantum well studied here. The generation of coherent phonons is resonantly enhanced when two exciton lines with the splitting tuned to the phonon energy are simultaneously excited; such a tuning is achievable by the quantum-confined Stark effect, where the exciton lines are shifted by varying the electric bias. However, there is also a strong emission of incoherent LO phonons due to intersubband transitions of the excited carriers; even in the resonant case this by far dominates the energy transfer to the lattice. The different contributions of the impulsive and the resonant coherent phonon generation mechanism are discussed. A good agreement with recent experiments is found.

DOI: 10.1103/PhysRevB.81.205320 PACS number(s): 63.20.kd, 73.21.Fg, 78.20.Bh

I. INTRODUCTION

By using ultrashort laser pulses coherent phonon oscillations can be excited in semiconductors.[1–5] The generation process is of an indirect nature, since the laser typically only affects the electronic degrees of freedom, which then, in turn, drive the lattice vibrations. Therefore this process can approximately be divided into two steps. In a first step the laser pulse excites the electronic subsystem on a time scale that is assumed to be quasi-instantaneous to the much slower phonon subsystem. In a second step the electronic subsystem then excites phonons. In many cases the dynamics of the electronic subsystem after the pulse is not relevant for the generation of coherent phonons, which means that those are impulsively generated by the sudden change induced by the pulse.[6,7] An example for this impulsive phonon generation is the displacive excitation of coherent phonons (DECP) mechanism,[8] which is relevant for excitation above the band gap. In this mechanism the laser pulse excites carriers and thereby abruptly changes the equilibrium positions of the lattice ions. As a consequence, coherent oscillations of the lattice ions around their new equilibrium positions set in.

The situation is different if oscillations in the electronic subsystem are created. These can have a period on the same time scale as the phonon oscillation, which makes it possible to resonantly drive coherent phonons. Such an oscillation may arise through the coherent superposition of two material transitions, which leads to a quantum beat whose frequency is determined by the energy splitting of the transitions. This is similar to the coherent Raman excitation technique, where two laser pulses with different frequencies are mixed and create an oscillation with a frequency determined by the detuning of the lasers.[9] In both cases the generation of coherent phonons becomes resonantly enhanced if the frequency of the beat oscillation is tuned to the frequency of a phonon mode. For example, such an enhancement has been found for the generation of coherent longitudinal-optical (LO) phonons in semiconductor superlattices if the frequency of a Bloch oscillation is tuned to the LO-phonon frequency.[10–12] In a quantum well structure the same enhancement effect occurs if two exciton lines with a splitting tuned to the energy of the LO phonon are simultaneously excited.[13,14] In this case the resulting electronic polarization resonantly drives coherent phonons, which has been observed both by tracing the time-resolved reflectivity[13] and by measuring terahertz emission.[14] The measured enhancement was quite strong: the amplitude of the phonon oscillation was increased by a factor of 20 and 10, respectively, in comparison to the nonresonant (DECP-like) case.

Related studies have been devoted to the generation of coherent acoustic phonons in a GaAs/AlAs nanostructure under electric bias driven by an electric current.[15,16] In contrast to the generation mechanisms discussed in this paper, the coherence of the phonons there does not arise through a coherent excitation process but through stimulated emission by the decay of incoherent LO phonons.

In this paper, we will analyze the resonant phonon generation (RPG) mechanism from a theoretical point of view. We employ a microscopic model of a semiconductor quantum well where the electronic degrees of freedom are coupled to the phonons via the Fröhlich interaction.[17] Based on this model, we will present simulations of the coherent phonon generation calculated using density-matrix theory. We will show that this model well reproduces the main features of the mechanism: the resonance in the splitting energy as well as the characteristic dependence on the central pump frequency and on the pump intensity. Our results are in good agreement with experimental findings.[13,14] Because in resonance the subband splitting is necessarily high enough such that intersubband relaxation processes by emission of incoherent phonons can take place, incoherent phonons are taken into account as well treated on a fully quantum kinetic level. We find that even in the case of resonantly enhanced generation of coherent phonons the energy transfer to incoherent phonons is much larger than to coherent phonons.

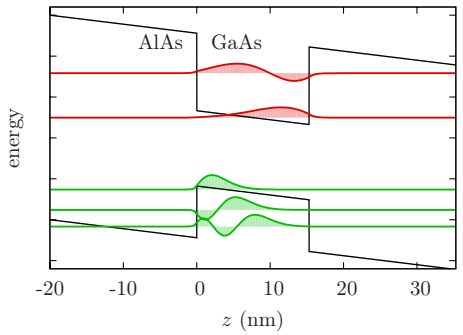

FIG. 1. (Color online) Schematic plot of the subband structure: potential well, energy levels, and wave functions (not drawn to scale). The wave functions refer to a bias field of 110 kV/cm.

II. MICROSCOPIC MODEL AND GENERATION MECHANISM

We use a model of a single GaAs/AlAs quantum well under an electric bias. Here, the bias voltage serves a double purpose. First, it leads to a charge separation between electrons and holes giving rise to an electrical dipole moment that may drive coherent phonons. Second, it can be used to tune the excitonic energy levels via the quantum-confined Stark effect (QCSE).[18] The parameters of the well are adjusted to model the structure used in the experiment of Ref. 13; there, a multiple quantum well has been used, where, however, tunneling between the wells is negligible and therefore all the wells behave independently. The confinement is modeled as a square potential tilted by the electric field. We assume a width of 15.3 nm and a total potential depth of 1.58 eV distributed 60/40 to conduction and valence bands, respectively. We limit our calculations to the lowest two electron subbands and the uppermost three heavy-hole subbands. A sketch of the subband structure of the quantum well including the respective envelope wave functions of electrons and holes is shown in Fig. 1 for the case of an electric field of 110 kV/cm.

The Hamiltonian for noninteracting electrons, holes, and LO phonons is given by

$$H_0 = \sum_{i,\mathbf{k}} \varepsilon^{\mathrm{e}}_{i\mathbf{k}} c^{\dagger}_{i\mathbf{k}} c_{i\mathbf{k}} + \sum_{j,\mathbf{k}} \varepsilon^{\mathrm{h}}_{j\mathbf{k}} d^{\dagger}_{j\mathbf{k}} d_{j\mathbf{k}} + \sum_{\mathbf{q}} \hbar\omega_{\mathrm{LO}} b^{\dagger}_{\mathbf{q}} b_{\mathbf{q}}, \quad (1)$$

where $c^{\dagger}_{i\mathbf{k}}(c_{i\mathbf{k}})$ denotes the creation (annihilation) operator for an electron in the ith subband with in-plane (two-dimensional) wave vector $\mathbf{k}$. Accordingly, $d^{\dagger}_{j\mathbf{k}}$ and $d_{j\mathbf{k}}$ are the hole creation and annihilation operators while $b^{\dagger}_{\mathbf{q}}(b_{\mathbf{q}})$ creates (annihilates) a phonon with the three-dimensional wave vector $\mathbf{q}$. The single-particle energy of an electron (hole) in the nth subband with wave vector $\mathbf{k}$ is denoted by $\varepsilon^{\mathrm{e(h)}}_{n\mathbf{k}}$ and the LO-phonon energy $\hbar\omega_{\mathrm{LO}}$ is taken to be constant.

To this Hamiltonian we add the interaction with the electric field $\mathbf{E}(t)$ of the laser pulse treated in the usual dipole approximation

$$H_{\mathrm{CF}} = \sum_{i,j,\mathbf{k}} [-\mathbf{E}\cdot\mathbf{M}_{ij} c^{\dagger}_{i\mathbf{k}} d^{\dagger}_{j-\mathbf{k}} - \mathbf{E}\cdot\mathbf{M}^{*}_{ij} d_{j-\mathbf{k}} c_{i\mathbf{k}}] \quad (2)$$

with the interband dipole matrix

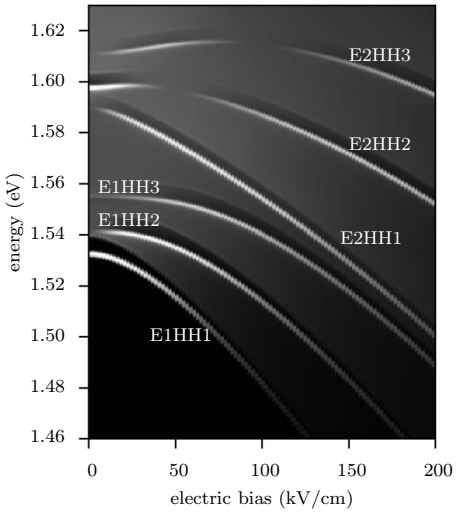

FIG. 2. Calculated absorption as a function of the photon energy and the electric bias field.

$$\mathbf{M}_{ij} = \mathbf{M}_0 \int \phi^{\mathrm{e}*}_i(z)\phi^{\mathrm{h}}_j(z)dz. \quad (3)$$

$\mathbf{M}_0$ is the common bulk part of the interband dipole matrix elements and $\phi^{\mathrm{e(h)}}_n(z)$ is the electron (hole) envelope wave function in the nth subband. A direct coupling to intraband transitions has been neglected as this is not relevant for excitation with an optical laser pulse.

We also include electron-electron interaction on the Hartree-Fock level in order to account for excitonic effects. Higher order terms like carrier-carrier scattering are neglected because we will restrict ourselves to comparatively low-carrier densities on the order of 10^{10} cm^{-2} where the scattering is dominated by LO-phonon emission. The Hamiltonian is not shown explicitly here, for details the reader is referred to, e.g., Ref. 17.

Based on this model we can calculate absorption spectra as a function of the bias electric field. The results are shown in Fig. 2. Standard material parameters for GaAs and AlAs have been used.[19] EnHHm labels the exciton line associated with the transition from the mth heavy-hole subband to the nth electron subband. At zero electric field all transitions but E1HH1 and E2HH2 are suppressed. The E1HH2, E2HH1, and E2HH3 transitions are forbidden due to symmetry while the E1HH3 transition has a negligible oscillator strength. With increasing bias these other transitions become allowed; the exciton lines change in strength and are shifted due to the QCSE. We are, in particular, interested in the E2HH1 and the E2HH2 exciton lines; their splitting approaches the LO-phonon energy at a bias field of about 110 kV/cm. These results agree qualitatively well with the photocurrent measurements of Ref. 13.

So far we have not included the interaction between LO phonons and charge carriers. In a polar semiconductor the dominant electron-phonon interaction is typically the Fröhlich coupling. Its Hamiltonian is given by[17,20]

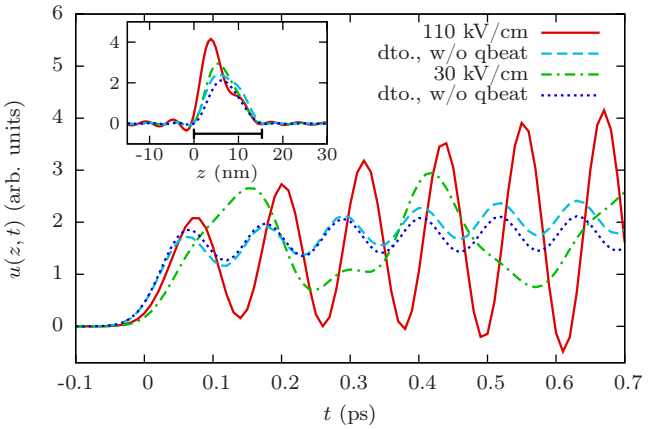

FIG. 3. (Color online) Lattice displacement field $u(z_0,t)$ versus t for resonant (solid curve, electric bias 110 kV/cm) and off-resonant conditions (dashed-dotted curve, 30 kV/cm); for each curve, z_0 is the position at which the oscillation is strongest. The dashed and dotted curves are the results of calculations where the off-diagonal elements of the electron and hole density matrices have been switched off. The inset shows $u(z,t_0)$ versus z, where t_0 is the time of the largest displacement; the horizontal bar indicates the extent of the quantum well.

$$H_{\mathrm{Fr}} = \sum_{\substack{i_1,i_2\\ \mathbf{k},\mathbf{q}}} [g_{\mathbf{q}}^{i_1 i_2} c_{i_1\mathbf{k}+\mathbf{q}_\parallel}^\dagger c_{i_2\mathbf{k}} b_{\mathbf{q}} + g_{\mathbf{q}}^{*i_1 i_2} c_{i_2\mathbf{k}}^\dagger c_{i_1\mathbf{k}+\mathbf{q}_\parallel} b_{\mathbf{q}}^\dagger] - \sum_{\substack{j_1,j_2\\ \mathbf{k},\mathbf{q}}} [g_{\mathbf{q}}^{j_2 j_1} d_{j_1\mathbf{k}+\mathbf{q}_\parallel}^\dagger d_{j_2\mathbf{k}} b_{\mathbf{q}} + g_{\mathbf{q}}^{*j_2 j_1} d_{j_2\mathbf{k}}^\dagger d_{j_1\mathbf{k}+\mathbf{q}_\parallel} b_{\mathbf{q}}^\dagger] \quad (4)$$

with $\mathbf{q}_\parallel$ and q_z being the in-plane and the z component of the wave vector $\mathbf{q}$, respectively. Here $g_{\mathbf{q}}^{n_1 n_2}$ is the Fröhlich matrix element defined as $g_{\mathbf{q}}^{n_1 n_2} = g_{\mathbf{q}}^{\mathrm{3D}} \mathcal{F}_{q_z}^{n_1 n_2}$ with the bulk Fröhlich matrix element

$$g_{\mathbf{q}}^{\mathrm{3D}} = -i\sqrt{\frac{e^2\hbar\omega_{\mathrm{LO}}}{2\varepsilon_0 V}\left(\frac{1}{\varepsilon_\infty}-\frac{1}{\varepsilon_s}\right)}\frac{1}{q}, \quad (5)$$

and the form factor

$$\mathcal{F}_{q_z}^{n_1 n_2} = \int \phi_{n_1}^*(z)\phi_{n_2}(z)e^{iq_z z}dz, \quad (6)$$

where V is the normalization volume, e is the elementary charge, ε_0 is the electric constant, and ε_s and ε_∞ are the static and optical dielectric constants. The operators $b_{\mathbf{q}}^\dagger$ and $b_{\mathbf{q}}$ create and annihilate bulk phonons with the wave vector $\mathbf{q}$. We have not assumed different phonon parameters for the AlAs part of the structure; first, we will see that because of the confinement of the electrons the lattice displacement is negligible outside the quantum well (cf. inset of Fig. 3), and second, phonon confinement effects become smaller with increasing quantum well width and should be insignificant for a relatively large width as the one considered here.[21]

Our model does not include phonon-phonon scattering. The LO phonon dephasing time in GaAs at low temperatures has been measured as $T_2/2 \approx 9$ ps,[22] so this is a legitimate approximation on the short time scales discussed in this paper. In fact, in the reflectivity measurements of Ref. 13 the decay is barely visible over a time of 3 ps.

The operator of the lattice displacement is connected to the phonon operators via

$$\hat{\mathbf{u}}(\mathbf{r}) = \sqrt{\frac{\hbar}{2M_r\omega_{\mathrm{LO}}N}}\sum_{\mathbf{q}}\frac{\mathbf{q}}{q}[b_{\mathbf{q}}^\dagger e^{-i\mathbf{q}\cdot\mathbf{r}} + b_{\mathbf{q}}e^{i\mathbf{q}\cdot\mathbf{r}}]. \quad (7)$$

Here M_r is the reduced mass of the lattice ions and N is the number of unit cells in the system volume. Coherent phonons are characterized by a nonvanishing expectation value of the displacement vector $\langle\hat{\mathbf{u}}(\mathbf{r})\rangle$ and thus a nonvanishing value of the coherent phonon amplitudes $\langle b_{\mathbf{q}}\rangle$. Because of the symmetry of the system the expectation value of the lattice displacement is zero in all directions but the z direction, that is, $\langle b_{\mathbf{q}}\rangle$ vanishes if $\mathbf{q}$ has a nonvanishing in-plane component. Using the density-matrix formalism we obtain the following equation of motion for the coherent phonon amplitude $B_{q_z} = \langle b_{q_z\mathbf{e}_z}\rangle$:

$$i\hbar\frac{d}{dt}B_{q_z} - \hbar\omega_{\mathrm{LO}}B_{q_z} = 2\sum_{i_1 i_2\mathbf{k}} g_{q_z}^{*i_1 i_2}\langle c_{i_2\mathbf{k}}^\dagger c_{i_1\mathbf{k}}\rangle - 2\sum_{j_1 j_2\mathbf{k}} g_{q_z}^{*j_2 j_1}\langle d_{j_2\mathbf{k}}^\dagger d_{j_1\mathbf{k}}\rangle. \quad (8)$$

The factor of 2 arises because we have implicitly summed over the spin degree of freedom.

The optical excitation affects the driving terms on the right-hand side of the equation on a time scale that is shorter than the oscillation period of the LO phonon. Let us first take a look at the impulsive, DECP-like part of phonon generation, which is related to the diagonal terms $\langle c_{n\mathbf{k}}^\dagger c_{n\mathbf{k}}\rangle$ and $\langle d_{n\mathbf{k}}^\dagger d_{n\mathbf{k}}\rangle$. Leaving aside excitonic and polaronic effects for a moment, these terms, i.e., the population of the electronic states, are constant after the pulse. In a simple approximation we can therefore assume that B_{q_z} is driven by an electronic population with a steplike time dependence. Solving the equation for $B_{q_z}(t)$ and substituting the result into Eq. (7) yields a lattice displacement whose time dependence is proportional to $[1-\cos(\omega_{\mathrm{LO}}t)]$. This cosinelike dependence is characteristic for the bulk DECP mechanism as well.[6] Physically, the new carrier distribution means a sudden shift of the equilibrium position of the lattice ions. The ions then start to oscillate around their new equilibrium. Obviously the amplitude of the coherent phonon oscillation is proportional to the number of carriers excited and thus—as long as phase-space filling effects are negligible—proportional to the integrated pump intensity.

For the resonant phonon generation mechanism the off-diagonal terms $\langle c_{n\mathbf{k}}^\dagger c_{n'\mathbf{k}}\rangle$ and $\langle d_{n\mathbf{k}}^\dagger d_{n'\mathbf{k}}\rangle$ with $n \neq n'$ are important. They signify a coherent superposition of two electron or two hole energy levels. If such a superposition is created, the resulting carrier density oscillates with a frequency determined by the splitting of the levels: the driving terms of Eq. (8) are proportional to $\exp(-i\omega_{nn'}t)$ where $\hbar\omega_{nn'}$ is the energy difference between the levels n and n'. Thus, B_{q_z} may be driven resonantly by tuning the splitting of two energy levels to the LO-phonon energy. In the present structure such

a resonance can be achieved for the first and the second hole subband at a bias field of about 110 kV/cm. To excite the coherent superposition, a short pump pulse with a spectral width which is broad enough to extend over both levels is needed. The superposition is strongest if the central energy of the pulse is chosen in a way that both levels are equally populated; if the transition matrix element is similar for both levels, the central energy should therefore lie in the center of the two levels. So the characteristics of the RPG mechanism are a resonant enhancement of the coherent phonon generation when the level splitting agrees with the LO-phonon energy and also a resonance behavior when the pump central energy comes close to the center of the two energy levels. Again the oscillation amplitude is proportional to the integrated pump intensity. Experimental evidence exists for both kinds of resonances as well as for the pump power dependence.[13,14]

In the discussion presented above we have oversimplified a few points. Coulomb interaction leads to the appearance of excitonic signatures, so, in fact, the coherent superposition will consist not only of two subbands but also of two exciton lines. In addition, we have not considered incoherent phonons. For resonance conditions a level splitting equal to the phonon energy is needed, which means that the carriers can make a transition from the upper to the lower level by emission of incoherent phonons. In fact, in the experiments a fast dephasing of the quantum beat has been observed[13,23] which, in part, can be attributed to this process.

In the density-matrix formalism carrier-phonon interaction gives rise to an infinite hierarchy of equations of motion for higher-order density matrices.[17] Coherent phonons appear on the first level of approximation if phonon-assisted density matrices like $\langle c^{\dagger}_{i\mathbf{k}} c_{i'\mathbf{k}'} b_{\mathbf{q}} \rangle$ are factorized into products of electronic density matrices and coherent phonon amplitudes such as $\langle c^{\dagger}_{i\mathbf{k}} c_{i'\mathbf{k}'} \rangle \langle b_{\mathbf{q}} \rangle$. Incoherent phonons and electron-phonon scattering processes appear on the next level by keeping the correlated part of the phonon-assisted density matrices like $\delta\langle c^{\dagger}_{i\mathbf{k}} c_{i'\mathbf{k}'} b_{\mathbf{q}} \rangle = \langle c^{\dagger}_{i\mathbf{k}} c_{i'\mathbf{k}'} b_{\mathbf{q}} \rangle - \langle c^{\dagger}_{i\mathbf{k}} c_{i'\mathbf{k}'} \rangle \langle b_{\mathbf{q}} \rangle$ and factorizing doubly phonon assisted terms, i.e., terms of the form $\langle c^{\dagger}_{i\mathbf{k}} c_{i'\mathbf{k}'} b_{\mathbf{q}} b_{\mathbf{q}'} \rangle$. We then obtain a closed set of equations of motion where in addition to the coherent phonon amplitudes higher order phonon variables like $\delta\langle b^{\dagger}_{\mathbf{q}} b_{\mathbf{q}'} \rangle = \langle b^{\dagger}_{\mathbf{q}} b_{\mathbf{q}'} \rangle - \langle b^{\dagger}_{\mathbf{q}} \rangle \langle b_{\mathbf{q}'} \rangle$ and $\delta\langle b_{\mathbf{q}} b_{\mathbf{q}'} \rangle = \langle b_{\mathbf{q}} b_{\mathbf{q}'} \rangle - \langle b_{\mathbf{q}} \rangle \langle b_{\mathbf{q}'} \rangle$ have to be calculated. We will refer to this level as a calculation of second order in the correlation expansion, whereas factorizing the single-phonon assisted terms will be called a first-order calculation.

III. NUMERICAL SIMULATIONS OF THE FULL MODEL

Let us now turn to simulations using this model. The quantum well has already been described. The electric field is varied from 0 to 160 kV/cm, which yields a splitting of the E2HH1 and the E2HH2 exciton lines between 8 and 46 meV (cf. Fig. 2). At 110 kV/cm the splitting approaches the LO-phonon energy of 36.3 meV. The pump pulse has a central energy of 1.571 eV, which is slightly above the center of the exciton lines in resonance, and a Gaussian shape with full width at half maximum (FWHM) of 100 fs corresponding to a spectral FWHM of 36 meV. Its intensity is fixed to a value that creates a carrier density in the well of about 10^{10} cm^{-2} at 110 kV/cm. Initial state is the thermal equilibrium at zero temperature.

Figure 3 shows the lattice displacement $u(z_0,t) = \langle \hat{u}_z(z_0,t) \rangle$ created by a pump pulse centered at $t=0$ for two different values of the bias field, 110 kV/cm corresponding to a resonance between exciton line splitting and LO-phonon frequency and 30 kV/cm, where the exciton line splitting is much smaller than the LO-phonon frequency. Here, z_0 refers to the position at which the oscillation is strongest; it has been determined independently for each curve. Let us first look at the results of calculations where the electronic quantum beats, i.e., the off-diagonal elements of the electron and hole density matrices, have been switched off by hand (dotted and dashed lines in Fig. 3). At both values of the bias field we find that the pulse initiates a nonvanishing lattice displacement which subsequently exhibits an oscillatory behavior. The oscillation frequency is given by the LO-phonon energy. This is exactly what is expected in the case of the DECP mechanism. Indeed, also the phase of the oscillations is in both cases in good agreement with the expected cosine-like behavior. In the resonant case we observe a slight increase in the mean value of the displacement with increasing time which results from a change in the electronic charge distribution caused by intersubband relaxation from the HH2 to the HH1 subband and from the E2 to the E1 subband associated with LO-phonon emission processes. At 30 kV/cm the heavy-hole subband splitting is much lower than the LO-phonon frequency, therefore such intersubband transitions are only possible for a small fraction of the holes in the high-energy tail of the distribution and for electrons in the E2 subband which, however, is only weakly excited in this case.

When including the electronic quantum beats the switching-on of the lattice displacement characteristic for the DECP mechanism is still present. The oscillations afterwards, however, are strongly modified. In the resonant case (at 110 kV/cm) the subband splitting matches the LO-phonon energy. Thus, a quantum beat in the electron-hole system oscillating with the LO-phonon frequency is excited. We observe that in this case the oscillation amplitude of the lattice displacement increases with time, which is a clear signature of a resonantly driven harmonic oscillator. Due to the periodic driving the phase of the oscillations is shifted compared to the DECP result. In the off-resonant case (at 30 kV/cm) the splitting is reduced to 15 meV, so the electronic quantum beat is much slower. We now have a nonresonantly driven harmonic oscillator and the lattice displacement exhibits oscillations with both the driving frequency and its own characteristic frequency ω_{LO}. Because of the off-resonant driving the amplitude is only modulated by the quantum beat but does not increase with time substantially.

In the inset of Fig. 3 the position dependence of the lattice displacement at a fixed time t_0 is shown. Again t_0 is the time when the displacement is largest, determined separately for each curve. The displacement is almost completely confined to the extent of the quantum well and its integral over the z direction does not vanish, which is possible because the electric field breaks the symmetry. Thus the coherent phonon

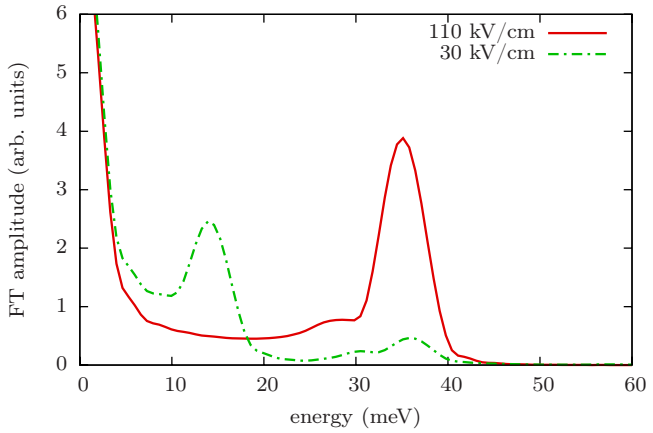

FIG. 4. (Color online) Spectral distribution of the coherent phonon oscillations at two different values of the bias field.

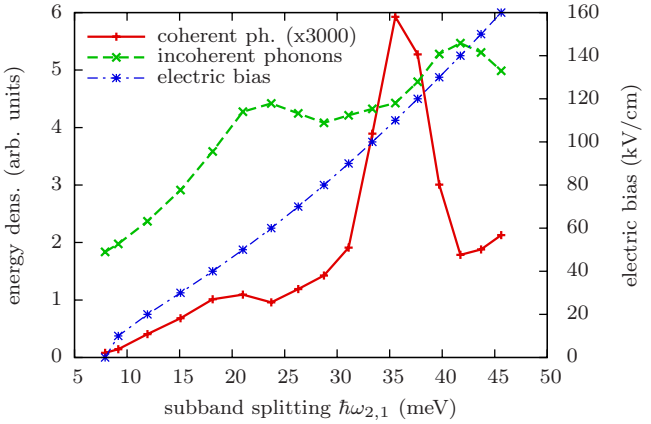

FIG. 5. (Color online) Time-averaged energy density contained in coherent and incoherent phonons versus the splitting between the HH1 and the HH2 subbands. The coherent phonon contribution is magnified by a factor of 3000. The dashed-dotted line shows the electric field strength corresponding to a given subband splitting.

oscillations are associated with a macroscopic dipole moment which gives rise to the emission of terahertz radiation as observed in the experiments.[14] In the resonant case the maximum of the displacement lies closer to the left side of the well because the wave functions associated with the heavy-hole subbands which drive the phonon oscillation are shifted toward this side (cf. Fig. 1).

Figure 4 shows the spectra of the coherent phonon oscillations at bias fields of 110 and 30 kV/cm obtained by Fourier transformation of the coherent phonon amplitude $u(z_0,t)$. We clearly see the behavior explained above. In both cases there is a low-frequency contribution resulting from the nonzero mean value of the displacement. Under resonance condition we have a strong single peak at the LO-phonon frequency while for an off-resonant driving of the coherent phonons two or more peaks are present. One is still at the LO-phonon frequency and the others are at the driving frequencies, i.e., the frequencies corresponding to the subband splittings. In the present case we have two such peaks, a large one resulting from the HH1-HH2 subband splitting at 15.1 meV and additionally a weak one at 29.3 meV due to the HH1-HH3 subband splitting.

We have seen that the amplitude of the coherent phonon oscillation is much larger when the quantum beat is tuned to the phonon frequency. We will now quantify this resonant enhancement by the amount of energy transferred to the coherent phonons, which is shown by the solid lines in Figs. 5 and 6 as a function of the subband splitting (Fig. 5) and the central pump frequency (Fig. 6), respectively. In order to account for all of the energy leaving the electronic subsystem, in addition to the free coherent phonon energy $\Sigma_{q_z}\hbar\omega_{\mathrm{LO}}|B_{q_z}|^2$ we have included in this value the coherent part of the interaction energy, i.e., the factorized part of the expectation value of the Fröhlich Hamiltonian (4). As the energy contained in coherent phonons oscillates, the average over the time from the beginning of the calculation, where the energy densities are zero, up to $t=0.7$ ps has been taken. In addition, we have also plotted the energy transferred to the incoherent phonons (dashed lines). Again this contains both the free phonon part $\Sigma_{\mathbf{q}}\hbar\omega_{\mathrm{LO}}\delta\langle b_{\mathbf{q}}^{\dagger}b_{\mathbf{q}}\rangle$ as well as the correlated part of the Fröhlich interaction energy and has been averaged over time. Since the amount of energy transferred into coherent phonons turns out to be much smaller than for incoherent phonons, in both figures the value for coherent phonons has been multiplied by a factor of 3000.

The resonance character of the coherent phonon generation when varying the splitting energy between the HH1 and the HH2 subbands is demonstrated in Fig. 5. The splitting is varied by changing the strength of the electric bias as indicated by the dashed-dotted line. The resonant enhancement in the energy density of coherent phonons is clearly visible as a peak at the point where the splitting energy matches the LO-phonon energy of 36.3 meV. This agrees well with our understanding of the generation mechanism and also with the experimental results in Ref. 13.

The second characteristic of the RPG mechanism is the resonance in the central energy of the pump pulse, which is shown in Fig. 6. The dashed-dotted line in the background shows the calculated absorption spectrum, i.e., the imaginary part of the electric susceptibility $\chi(\omega)$; this spectrum, unlike

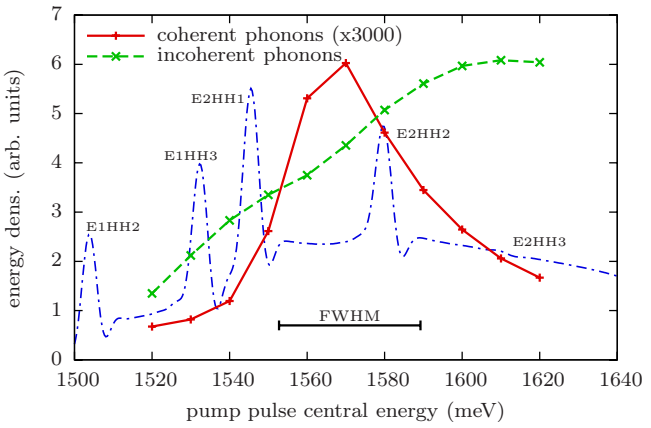

FIG. 6. (Color online) Time-averaged energy density contained in coherent and incoherent phonons versus the central energy of the pump pulse with the electric bias field fixed at 110 kV/cm. The dashed-dotted line shows the absorption spectrum calculated with polaron effects included and the horizontal bar indicates the spectral width of the pump pulse.

those shown in Fig. 2, includes the electron-phonon interaction and thereby accounts for polaron effects. The exciton peaks are labeled by their respective subbands. As expected, the generation of coherent phonons peaks between the E2HH1 and the E2HH2 line. It is not exactly in the center but slightly shifted toward the E2HH2 line. This is because the E2HH2 transition is weaker and because it is superimposed to the continuum part of the E2HH1 transition. This, too, matches the measurements of Ref. 13.

Even at resonance, however, we find that the energy stored in coherent phonons is about three orders of magnitude smaller than the energy stored in incoherent phonons. This means that intersubband relaxation strongly dominates the energy transfer from the electronic subsystem to the lattice. The dependence of the energy density of incoherent phonons on the subband splitting (Fig. 5) can be understood as follows. At zero-bias field essentially only the E1HH1 transition is excited. Because the central pump frequency is about 40 meV above the exciton resonance and because of the rather large spectral width intrasubband relaxation processes are possible for a considerable fraction of the excited electrons already here. With increasing bias field the exciton resonances shift to lower energies thus increasing the excess energy of the excited carriers. In addition, optical transitions to higher hole and electron subbands become allowed and thus phonon-induced intersubband transitions appear. Both phenomena lead to the increase in the energy density of incoherent phonons with increasing bias field. The two maxima superimposed on this general increase at subband splittings of about 23 and 42 meV are due to the fact that at the respective bias fields of 60 kV/cm and 140 kV/cm the central energy of the pump laser becomes resonant to the E2HH1 and the E2HH2 transitions, respectively, leading to maxima in the total generated carrier density (see Fig. 2). For the dependence on the pump energy (Fig. 6) we observe a similar behavior. The number of incoherent phonons generally increases with higher pump energy as more electrons are excited in higher-lying subbands which can relax down.

The ratio of the energy density of coherent and of incoherent phonons is increased at higher pump intensities: the energy density of coherent phonons depends quadratically on the coherent phonon amplitude and therefore increases with the square of the excited carrier density, while the energy density of incoherent phonons depends linearly on the carrier density. At low-pump intensities the carrier density increases linearly with the pump intensity. However it cannot be raised to arbitrarily large values due to phase-space filling; if this is taken into account we find that in the system considered here the energy transfer to incoherent phonons will always be dominant.

IV. CONCLUSIONS

We have presented a theoretical investigation of the resonant generation of coherent phonons in a quantum well under bias. In this mechanism a short optical excitation creates an electronic quantum beat. The oscillating charge distribution of electrons and holes associated with this quantum beat drives coherent phonons. The electric bias can be used to tune the splitting of two exciton lines to the phonon energy; at this point the generation becomes resonantly enhanced. This resonance as well as a resonance in the central energy of the pump pulse are characteristic for the mechanism. These properties can be directly inferred from the model system and have also been reproduced in numerical simulations. The results agree favorably with experiments. In the simulation incoherent phonons have been taken into account on a fully quantum kinetic level, as the resonant generation of coherent phonons is not possible without allowing for relaxation processes by emission of incoherent phonons. The numerical calculations show that only a very small part of the energy transferred from the electronic subsystem to the lattice goes into coherent phonons which give rise to measurable oscillations of the lattice displacement. The largest part excites incoherent phonons which only increase the fluctuations of the lattice displacement field.

ACKNOWLEDGMENT

Financial support of the DFG (Grant No. KU 697/11-1) is gratefully acknowledged.

*t.papenkort@uni-muenster.de

[1] G. C. Cho, W. Kütt, and H. Kurz, Phys. Rev. Lett. **65**, 764 (1990).
[2] R. Merlin, Solid State Commun. **102**, 207 (1997).
[3] K. J. Yee, K. G. Lee, E. Oh, D. S. Kim, and Y. S. Lim, Phys. Rev. Lett. **88**, 105501 (2002).
[4] A. V. Kuznetsov and C. J. Stanton, Phys. Rev. Lett. **73**, 3243 (1994).
[5] T. Pfeifer, T. Dekorsy, W. Kütt, and H. Kurz, Appl. Phys. A: Mater. Sci. Process. **55**, 482 (1992).
[6] K. J. Yee, Y. S. Lim, T. Dekorsy, and D. S. Kim, Phys. Rev. Lett. **86**, 1630 (2001).
[7] W. A. Kütt, W. Albrecht, and H. Kurz, IEEE J. Quantum Electron. **28**, 2434 (1992).
[8] H. J. Zeiger, J. Vidal, T. K. Cheng, E. P. Ippen, G. Dresselhaus, and M. S. Dresselhaus, Phys. Rev. B **45**, 768 (1992).
[9] W. E. Bron, J. Kuhl, and B. K. Rhee, Phys. Rev. B **34**, 6961 (1986).
[10] T. Dekorsy, A. Bartels, H. Kurz, K. Köhler, R. Hey, and K. Ploog, Phys. Rev. Lett. **85**, 1080 (2000).
[11] A. W. Ghosh, L. Jönsson, and J. W. Wilkins, Phys. Rev. Lett. **85**, 1084 (2000).
[12] M. Först, H. Kurz, T. Dekorsy, and R. P. Leavitt, Phys. Rev. B **67**, 085305 (2003).
[13] O. Kojima, K. Mizoguchi, and M. Nakayama, Phys. Rev. B **70**, 233306 (2004).
[14] M. Nakayama, S.-I. Ito, K. Mizoguchi, S. Sait, and K. Sakai, Appl. Phys. Express **1**, 012004 (2008).

[15] R. P. Beardsley, A. V. Akimov, M. Henini, and A. J. Kent, Phys. Rev. Lett. **104**, 085501 (2010).
[16] I. Camps, S. S. Makler, H. M. Pastawski, and L. E. F. Foa Torres, Phys. Rev. B **64**, 125311 (2001).
[17] F. Rossi and T. Kuhn, Rev. Mod. Phys. **74**, 895 (2002).
[18] D. A. B. Miller, D. S. Chemla, T. C. Damen, A. C. Gossard, W. Wiegmann, T. H. Wood, and C. A. Burrus, Phys. Rev. Lett. **53**, 2173 (1984).
[19] S. Adachi, *GaAs and Related Materials: Bulk Semiconducting and Superlattice Properties* (World Scientific, Singapore, 1994).
[20] T. Kuhn, in *Theory of Transport Properties of Semiconductor Nanostructures*, edited by E. Schöll (Chapman and Hall, London, 1998), pp. 173–214.
[21] D. Gammon, B. V. Shanabrook, and D. S. Katzer, Phys. Rev. Lett. **67**, 1547 (1991).
[22] F. Vallée and F. Bogani, Phys. Rev. B **43**, 12049 (1991).
[23] K. Mizoguchi, O. Kojima, T. Furuichi, M. Nakayama, K. Akahane, N. Yamamoto, and N. Ohtani, Phys. Rev. B **69**, 233302 (2004).